Proceedings World Geothermal Congress 2020+1
Reykjavik, Iceland, April - October 2021

Simulation of Gas Production from Hydrate Reservoirs with Geothermal Energy

Panpan ZHANG, Shouceng TIAN, Wenhong ZHANG, Yiqun ZHANG, Chao YU

Email: zhangpanpan0819@126.com

Keywords: Natural gas hydrate; Gas production simulation; Depressurization; Geothermal stimulation; The South China Sea;

ABSTRACT

Natural gas hydrate is a potential energy source, rich in resources, efficient, and environmentally friendly. However, low extraction efficiency is a monumental challenge for its industrial development. Recent studies show that some natural gas hydrate reservoirs in the South China Sea coexist with geothermal resources. Through the combination of two horizontal wells, geothermal energy is applied in the exploitation of hydrate. A numerical model is established to study the gas production behavior of GHBS by depressurization and geothermal stimulation. The hydrate extraction efficiency of the combination of geothermal stimulation and depressurization is compared with a control group without geothermal stimulation. Results indicate that the thermal stimulation effects are limited to the injection area well in the first 50 days. The development effect is positively related to the temperature at which hot water is injected. Besides, the under-injection up-production model is more conducive to the development of hydrates. This work provides some preliminary insights into the efficacy of hydrate exploitation with deep geothermal energy.

1. INTRODUCTION

Natural gas hydrates are solid, non-stoichiometric compounds of small gas molecules and water, which form when constituents coexist in environments of low temperatures and high pressures (Sloan 2003). In nature, the most abundant species of hydrates is methane hydrate, and it is widely distributed in the permafrost and the shallow sub-seafloor sediments (Chong et al. 2017; Yin et al. 2018b). The global estimates of methane trapped in hydrate range widely between 10^{15} and 10^{18} ST m^3, likely more remarkable than the total energy content of the known conventional fossil fuel resources (Moridis & Sloan 2007; Moridis et al. 2011; Fitzgerald & Castaldi 2013). As a clean alternative energy source in the future, the efficient development of natural gas hydrate is of great significance to issues such as meeting growing energy demand and promoting green developments (Li et al. 2016; Sun et al. 2019).

At present, the main hydrate recovery methods include depressurization, thermal stimulation, inhibitor injection, and CO_2 displacement (Yin et al. 2018a). Thermal stimulation and inhibitor injection have shown poor performance in zones far away from the injection well and relatively high costs (Reagan et al. 2015). Injecting inhibitors into oceanic hydrate deposits also brings about environmental concerns. CO_2 replacement can extract gas from CH_4 hydrate and obsess potential benefits of the maintenance of seafloor integrity, significant reduction in water production, and carbon storage. However, the continuous formation of CO_2 hydrate will seriously hinder long-term gas exchange (Koh et al. 2016; Li et al. 2018a). Among these methods, depressurization is relatively simple and efficient (Yang et al. 2016; Terzariol et al. 2017). Hydrate dissociation is an endothermic process that might lead to a sharp drop in temperature during depressurization, resulting in the self-preservation phenomenon (Chong et al. 2016b). Therefore, the combination of thermal stimulation and depressurization is regarded as a promising approach to enhance hydrate extraction efficiency by previous studies (Yang et al. 2014; Chong et al. 2016a).

In 2017, by depressurization in a vertical well, the China Geological Survey conducted the first production test of methane hydrate in a silty clay formation in the Shenhu area, the South China Sea. The production lasted for 60 days, with an average gas production rate higher than 5000 m^3/day. In 2020, by applying depressurization in a horizontal well and reservoir stimulation, the second hydrates extraction field trial in this area lasted 30 days. The average gas production rate set a world record of 2.87×10^4 m^3/day (Ye et al. 2020). However, it is much lower than the economic viability level, which is considered at least 5×10^5 m^3/day (Sloan 2003). In situ measurements indicate that the geothermal gradient in the Shenhu area is 4.3-6.7℃/100 m (Sun et al. 2015). Thus, it is possible to use geothermal energy to facilitate hydrate exploitation.

In this work, we carried out numerical simulations to investigate geothermal stimulation's influence on improving natural gas hydrate extraction efficiency. The heat carrier fluid is assumed to be water, heated in the geothermal formation, and then injected into the gas hydrate-bearing sediments (GHBS). We compared the multi-physical behaviors and productivity of GHBS in different situations. Also, we analyzed the influence of the temperature of injected water and well layout on hydrate extraction. In light of the previous work conducted by Liu et al. (Liu et al. 2018), this study gives some new insights into geothermal assisted gas hydrates development.

2. MODEL DESCRIPTION

2.1 Numerical simulation code

In this study, a two-dimensional model is constructed using an open-source simulator HydrateResSim (HRS), developed by the Lawrence Berkeley National Laboratory. Based on insights provided by TOUGH2/EOSHYDR2, fewer primary variables were selected, and more powerful linearization techniques were employed in HRS, resulting in significant improvement in execution speed and numerical performance (Moridis 2002). By solving coupled equations of mass and heat balance, HRS can deal with the non-isothermal gas release, phase behavior, and flow of fluids and heat at common conditions of natural methane hydrate accumulations (Moridis et al. 2005). Up to now, HRS has been widely used in simulations of gas production from GHBS induced by depressurization and thermal stimulation (Hou et al. 2016; Zheng et al. 2018; Lu et al. 2019).

2.2 Hydrates deposits in the South China Sea

The two-dimensional model is constructed based on the geological data from the SH7 site in the Shenhu area of the South China Sea (Li et al. 2013), which is recognized as one of the most promising gas hydrate deposits. The hydrate accumulations in this area are similar to Class 3 deposits, involving only hydrate-bearing sediments but without impermeable overburden and underburden. Drilling results indicate that the top of the hydrate layers located at 155-229 m below the seafloor, with layer thickness ranging from 10 m to 43 m and water depth varying from 1108 m to 1245 m. Estimates of sediment porosity and hydrate saturation are from 33%-48% and 26%-48%, respectively. Detailed geological data in this area can be found in previous studies (Xu & Li 2015; Li et al. 2018b).

2.3 Model construction

Fig. 1 shows a schematic of the geothermal assisted hydrate exploitation system. The injection well consists of a vertical wellbore and a horizontal branch, and the horizontal branch is parallel to the horizontal section of the production well. Water is injected into the geothermal formation through the injection well, heated during tubing-annulus flowing, and finally flowing into the GHBS. The bottom pressure of the production well is kept low to extract gas from GHBS. In this work, a plane perpendicular to the horizontal section of the production well and the injection well (marked in Fig. 1a) is selected for modeling, which has a unit thickness in the y direction.

Fig. 2 illustrates the schematic of the well layout and mesh design for gas production simulation. The model extends 50 m and 80 m in the x and z directions, respectively. The outer sides of the model (x = 0 and x = 50) are treated as no-flow boundaries. The thickness of GHBS is 20 m, and the thickness of overburden and underburden are both 30 m. As shown in Fig. 2, the model domain is discretized into 1519 (31 × 1 × 49) elements in a Cartesian coordinate system (x-y-z). For a better resolution in concerned areas, mesh around wellbores and boundaries are refined. The equivalent hydraulic radius of the injection and production wellbores is set to 10 cm by adjusting the grid size. Based on the model, six hydrate extraction schemes are designed (Table 1).

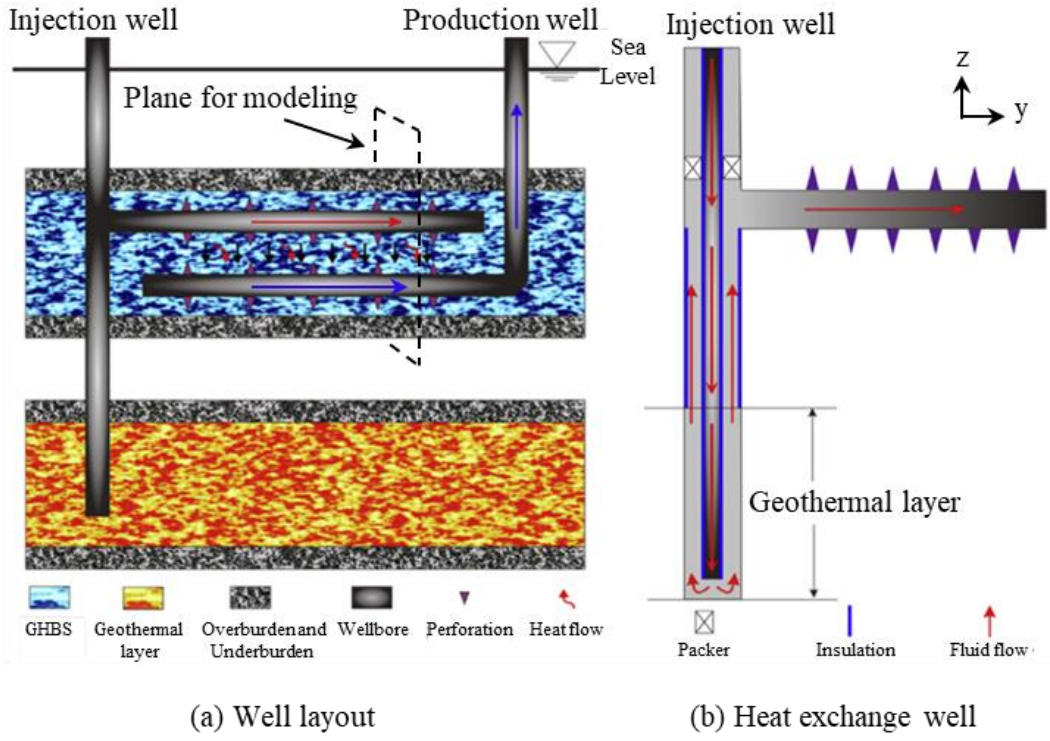

Fig. 1 A schematic of the geothermal assisted hydrate exploitation system (modified according to (Liu et al. 2018)).

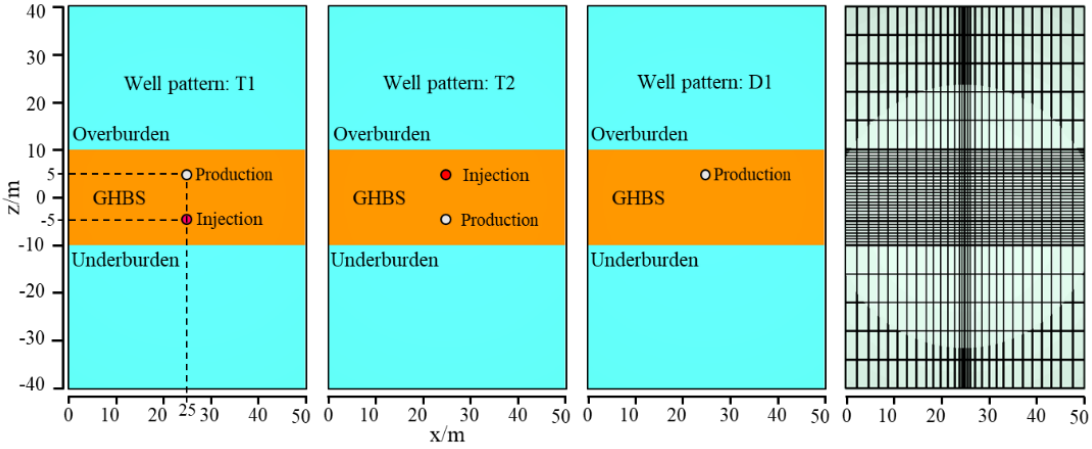

Fig. 2. Schematic of the well layout and mesh design for gas production simulation.

Table 1 Hydrate extraction schemes in this study.

Case	Temperature of injection water (℃)	Well Pattern
Case 1	No	D1
Case 2	20	T1
Case 3	30	T1
Case 4	40	T1
Case 5	50	T1
Case 6	50	T2

To avoid a theoretically correct but computationally intensive solution of the Navier–Stokes equation, we hypothesize the flow in the injection and production wellbores is Darcy flow. The wellbores have a porosity of 1.0, permeability Kx = Kz = 10^{-9} m^2, and no capillary pressure. Fig. 3 shows the initial condition of the simulation system. The uppermost and lowermost layers are defined as fix-state cells with constant pressure and temperature conditions to introduce the geothermal gradient. The distribution of temperature and pressure has reached a steady state (Fig. 3a and 3b) by preprocessing run, which is necessary for proper initiation. The initial pressure and temperature at the bottom of GHBS are 13.83 MPa and 14.15 ℃, respectively. In the beginning, the GHBS is saturated with hydrate and water. The overburden and underburden are fully saturated with water. The pressure of the heat injection well is set to 14 MPa, which is slightly higher than its surroundings. The pressure of the production well is set to 3 MPa, which is slightly higher than the quadruple point of methane hydrate to keep ice from forming, and the production lasts 500 days. More information about the simulation system is shown in Table 2.

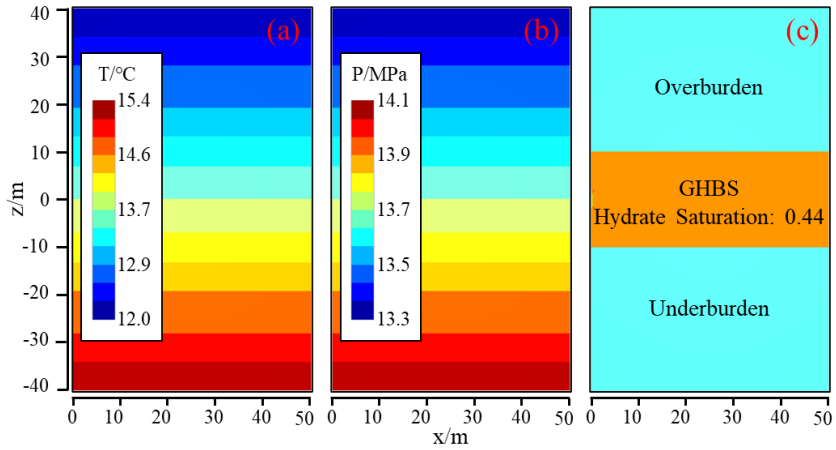

Fig. 3. Initial conditions of the simulation system

Table 2 Properties of hydrate deposit at site SH7 and parameters used in the numerical model. (Based on the report of (Li et al. 2010))

Parameter	Value	Parameter	Value
Overburden thickness	30 m	Reaction model	Equilibrium hydrate reaction
GHBS thickness	20 m	Gas composition	100% CH_4
Underburden thickness	30 m	Hydration number	6
Initial pressure P_B (at the base of GHBS)	13.83 MPa	Thermal conductivity model	$k_\theta = k_{dry} + \sqrt{S_A}(k_{wet} - k_{dry}) + \phi S_H k_H + \phi S_I k_I$
Initial temperature T_B (at the base of GHBS)	287.31 K (14.15 ℃)	Dry thermal conductivity k_{dry} (all formations)	1.0 W/(m·K)
Porosity ϕ (all formations)	0.41	Wet thermal conductivity k_{wet} (all formations)	3.1 W/(m·K)
Initial saturation in the overburden and underburden	S_W = 1.0	Intrinsic permeability of all formations	k_x=75 mD k_z= 20 mD
Initial saturation in GHBS	S_H = 0.44 S_W = 0.56	Relative permeability model	$k_{rA} = [(S_A - S_{irA})/(1 - S_{irA})]^n$ $k_{rG} = [(S_G - S_{irG})/(1 - S_{irG})]^{nG}$ $n = n_G = 3.572;\ S_{irA} = 0.3;\ S_G = 0.05$
Geothermal gradient	0.0433 K/m	Capillary pressure model	$P_{cap} = P_0\left[(S^*)^{-1/\lambda} - 1\right]^{1-\lambda}$ $S^* = (S_A - S_{irA})/(1 - S_{irA})$ $S_{irA} = 0.29;\ \lambda = 0.45;\ P_0 = 10^5$ Pa

3. RESULTS AND DISCUSSION

3.1 Spatial distribution of physical properties

For the convenience of analysis and comparison, Case 1 and Case 5 were selected as representatives of the vertical well and the radial wells, respectively. The spatial evolutions of hydrate saturation, gas saturation, and temperature Case 1 and Case 5 are shown in Figures 4-6. Analysis of the multi-physical behavior of GHBS is of significance to explain the gas production behaviors during depressurization and thermal stimulation.

3.1.1 Evolutions of the hydrate and gas saturation

Fig. 4 shows the spatial distribution of hydrate saturation on the 10th, 100th, and 500th day of Case 1 and Case 5. In the early stages, hydrate dissociation appears around the production well and heat injection well. It also occurs near the upper and lower interfaces of GHBS. Before the 100th day, the hydrate dissociation pattern around the production well of Case 1 and Case 5 are very similar. For Case 5, the hydrate decomposition area around the production is much broader, indicating that hydrate dissociation is mainly induced by depressurization. On the 500th day in Fig. 4, the hydrate extraction performance in Case 5 is better than in Case 3, especially in the lower part of GHBS.

Fig. 5 depicts the spatial distribution of gas saturation on the 10th, 100th, and 500th day of Case 1 and Case 5. On the 10th day of production, thermal stimulation is negligible in zones far away from the heat injection well, showing no influence on gas production behaviors. Notable differences in gas distribution are observed on the 100th day of Case 1 and Case 5. Gas areas induced by thermal stimulation and depressurization are connected, which means that extra gas would flow into the production well in Case 5. It can also be inferred that the thermal stimulation comes into effect earlier than the 100th day of production. On the 500th day of Case 5, the gas saturation around the production well and the injection well drops to an extremely low level. Whereas,

there is still abundant gas around the production well on the 500th day of Case 1. Therefore, the gas production cycle of Case 1 is expected to be longer than that of Case 5.

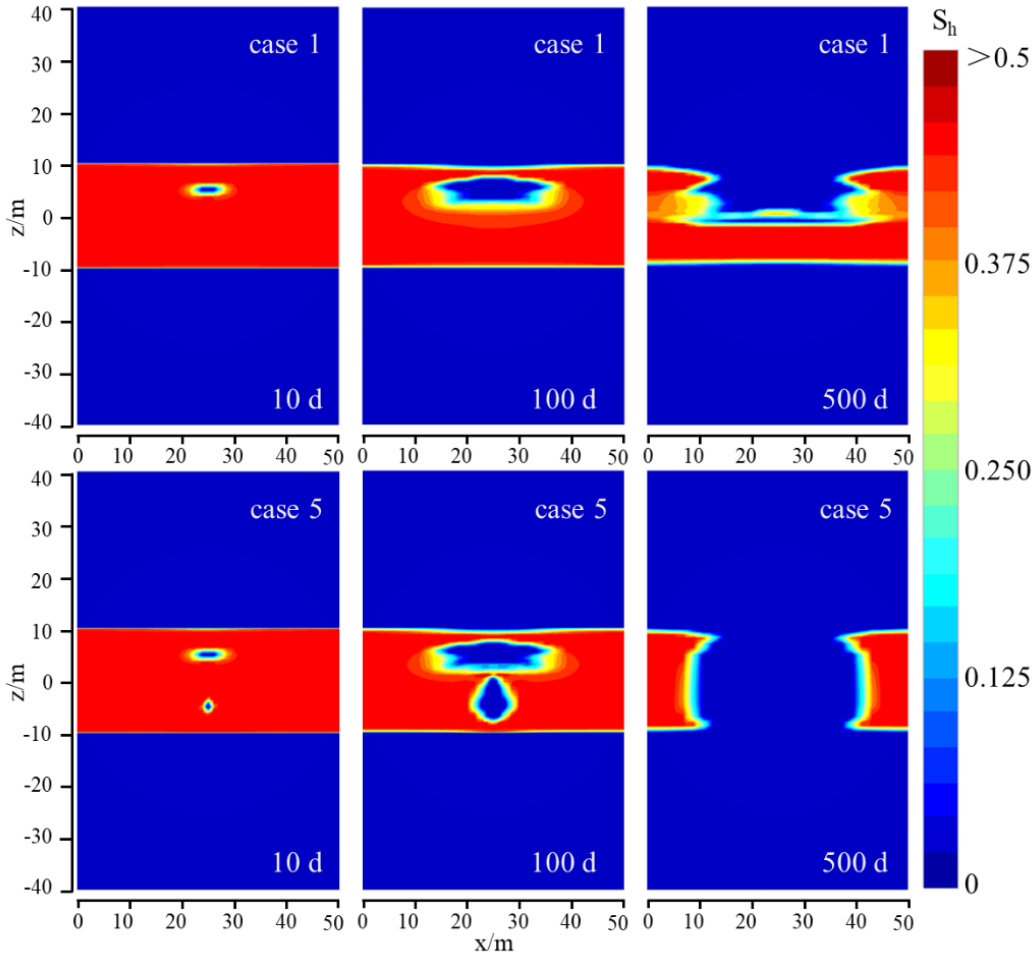

Fig. 4. Spatial distribution of hydrate saturation on the 10th, 100th, and 500th day of Case 1 and Case 5.

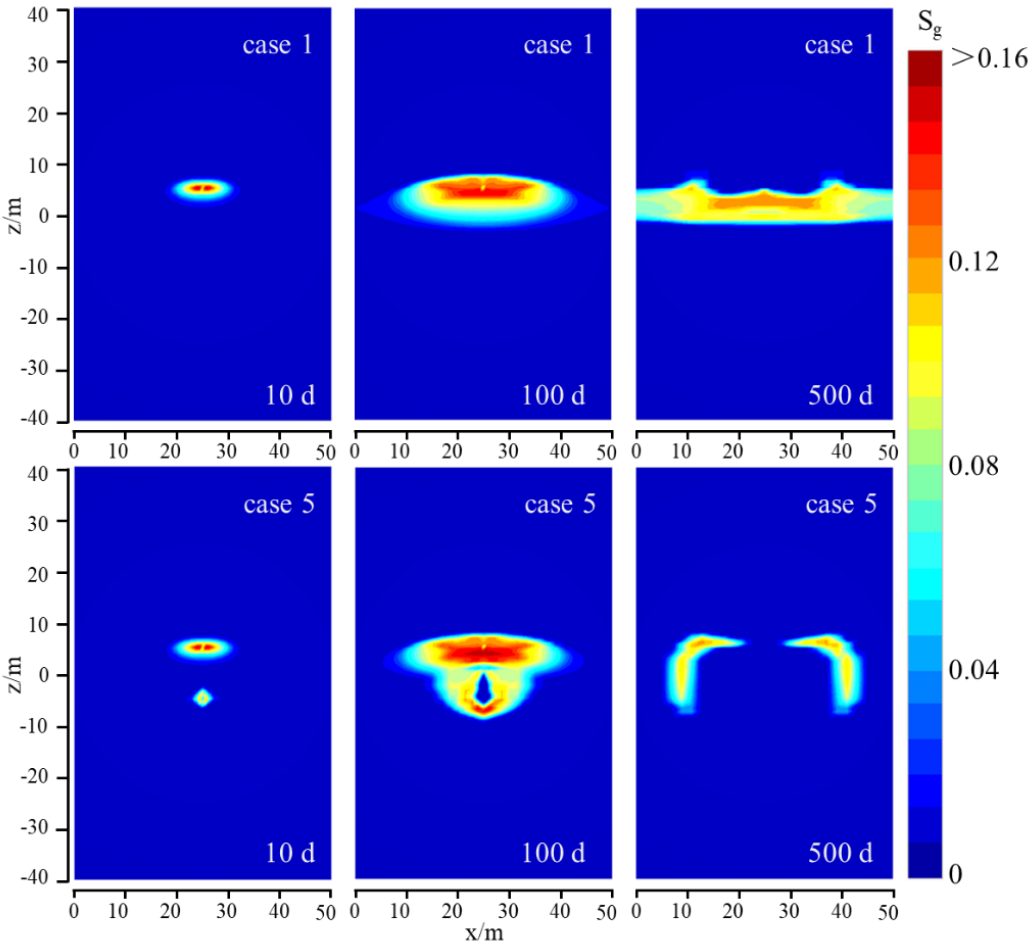

Fig. 5. Spatial distribution of gas saturation on the 10th, 100th, and 500th day of Case 1 and Case 5.

3.1.2 Spatial distribution of temperature

As mentioned before, hydrate dissociation is initially triggered by the depressurization and heat injection. The decomposition of hydrate is an endothermic process, which would cause temperature redistribution. Fig. 6 shows the temperature distribution of Case 1 and Case 5 during gas production, which closely matches the dissociation behavior of hydrate in Fig. 4. On the 10th day of Case 1 and Case 5, the decomposition of hydrate creates the low-temperature areas around the wellbore and the upper interface of GHBS. On the 100th day, enlarged low-temperature regions are observed in Case 1. With heat supply from the injection well, the low-temperature regions are relatively small. On the 500th day of Case 5, these regions disappeared because the local hydrate dissociation almost ceases. For Case 1, the temperature in the upper part of GHBS gradually recovers after the hydrate in this area is exhausted.

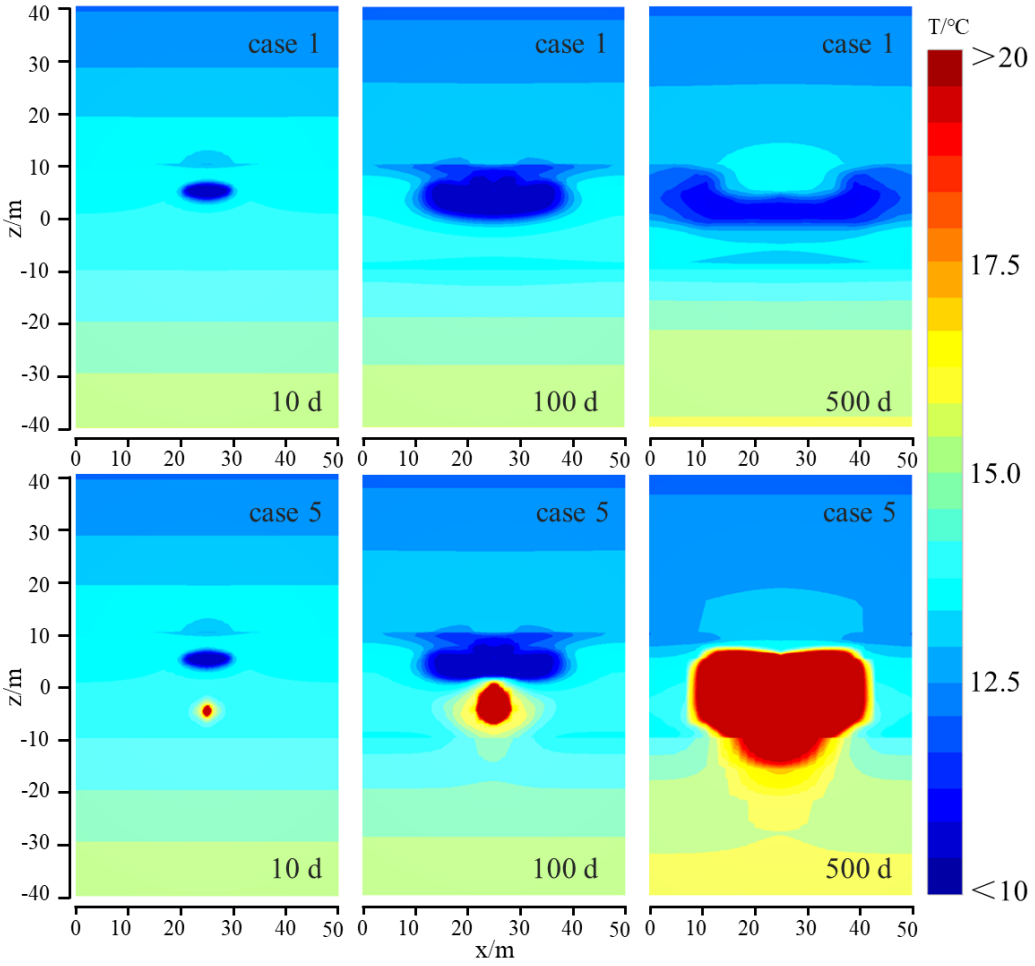

Fig. 6. Spatial distribution of temperature on the 10th, 100th, and 500th day of Case 1 and Case 5.

3.2 Productivity analysis

3.2.1 Sensitivity of the temperature of injection water

To clarify the influence of injection water temperature on enhancing hydrate extraction efficiency, the gas productivities of cases 1-5 are compared. Fig. 7 shows the changes in the gas production rate and cumulative gas production during the simulations of Case 1-5. As shown in Fig. 7a, the gas production rate curves of Case 1-5 almost coincide in the first 50 days. It is because that the hydrate decomposition front associated with the thermal stimulation has not yet reached the production wells. After the 50th day, the gas production rate curves begin to diverge, and the cases with higher temperatures of water injection tend to have higher gas production rates. Besides, the performance of Case 5 is much better than the other cases. As illustrated in Fig. 7b, the cumulative gas production of Case 5 with 50 ℃ water injection is more than 8000 m^3, which shows a 60% increase compared to Case 1 without heat injection. Fig. 7 indicates that in the early stages, the injection of heat water has little effect on gas production, which is well explained by the previous analysis on the multi-physical behaviors of GHBS. It is worth noting that the performance of Case 2 (20 ℃ water injection) in gas production is worse than Case 1 (without thermal stimulation). This may be because the temperature of injected water is so low that the pressure increase caused by water injection outweighs the benefits from thermal stimulation.

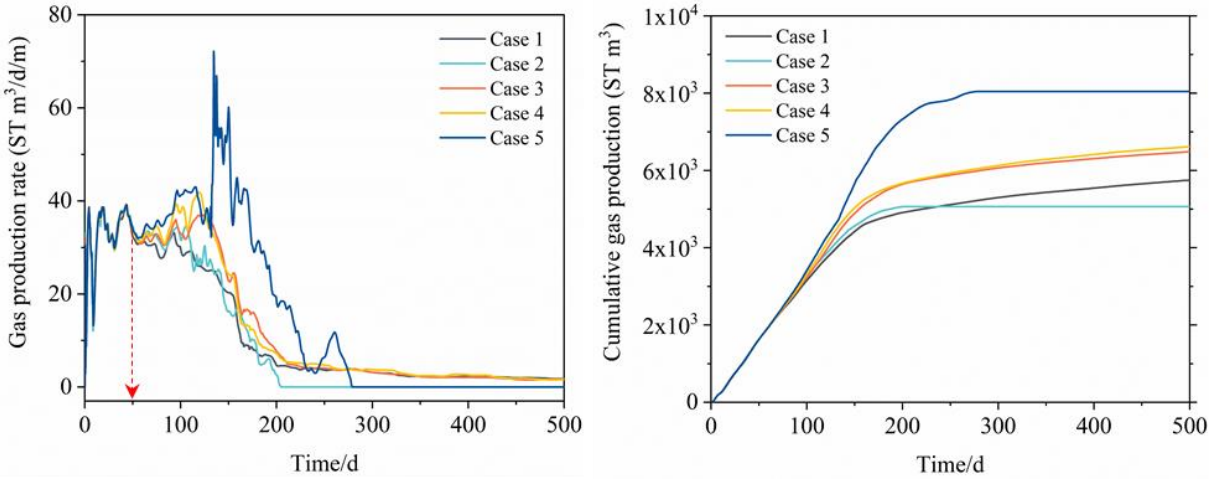

(a) **(b)**

Fig. 7. Evolution of the (a) gas production rate and (b) cumulative gas production of Case 1-5.

3.2.2 Influence of the well layout

The layout of the injection well and production well would also influence the productivity of GHBS. The injected water temperatures of Case 5 and Case 6 are the same, but the wells' layouts are opposite. The injection well of Case 5 is located below the production well (T1 pattern in Fig. 2). Fig. 8 shows the gas production rate and cumulative gas production of Case 5 and Case 6. It can be observed that the production performance of Case 5 is better than that of Case 6. The difference in the gas production rate of Case 5 and Case 6 enlarges after the 100th day (Fig. 8a). Although the total gas production of Case 5 and Case 6 is close, gas yields of Case 5 concentrated in the early stages, which was preferred in field tests.

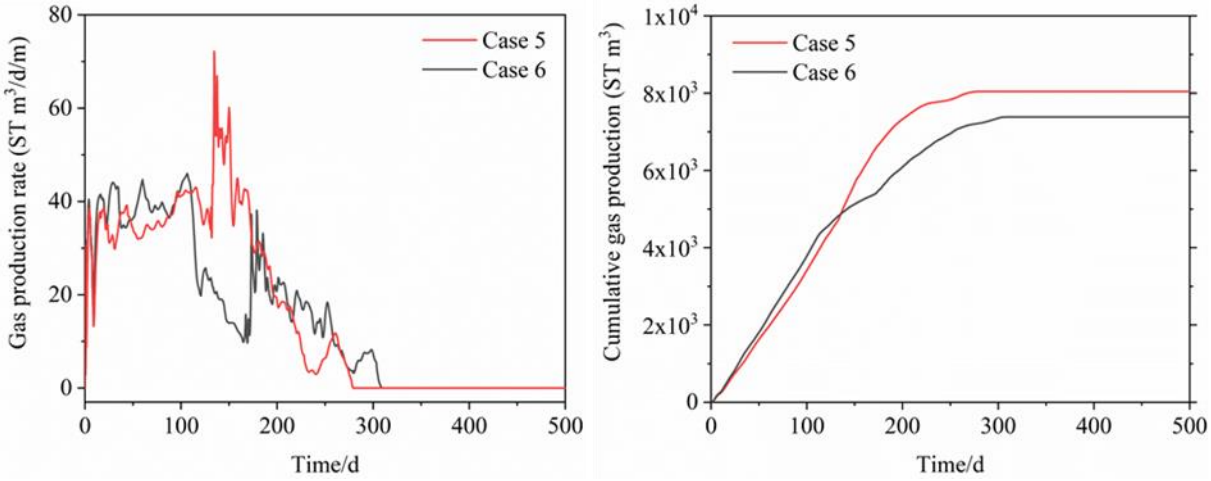

(a) **(b)**

Fig. 8. Evolution of the (a) gas release rate and (b) gas production rate of Case 3 and Case 5.

4. CONCLUSION

In this study, the combination of geothermal stimulation and depressurization is applied to exploit oceanic hydrate reservoirs in the South China Sea. A numerical model was constructed using an open-source simulator HRS to evaluate this method's efficacy. Some preliminary insights are obtained by analyzing the multi-physical behavior and productivity of GHBS.

（1）In the early stages, the effects of thermal stimulation are limited to the area around the injection well. About 50 days later, differences in gas production rate associated with thermal stimulation can be observed.

（2）There is a positive correlation between the development effect and the temperature at which hot water is injected. The total gas production of Case 5 with 50 ℃ water injection is more than 8000 m^3, which is 60% higher than that of Case 1 without heat injection. Thermal stimulation with relatively low-temperature water (20 ℃) would deteriorate the gas production performance.

（3）The gas production behaviors are sensitive to the layout of the heat injection well and the gas production well. The under-injection up-production model is more conducive to the development of hydrates.

ACKNOWLEDGMENTS

The authors would like to thank the National Energy Technology Laboratory from the U.S. Department of Energy for providing the simulator HydrateResSim. This work was financially supported by the National Natural Science Foundation of China (Grant Nos. 51804320, 51827804, and 51991362)

REFERENCES

Chong, Z., Pujar, G.A., Yang, M., et al. Methane hydrate formation in excess water simulating marine locations and the impact of thermal stimulation on energy recovery. Applied Energy, 177, (2016a), 409-421.

Chong, Z., Yang, S.H.B., Babu, P., et al. Review of natural gas hydrates as an energy resource: Prospects and challenges. Applied Energy, 162, (2016b), 1633-1652.

Chong, Z.R., Yin, Z., Tan, J.H.C., et al. Experimental investigations on energy recovery from water-saturated hydrate bearing sediments via depressurization approach. Applied Energy, 204, (2017), 1513-1525.

Fitzgerald, G.C., Castaldi, M.J. Thermal Stimulation Based Methane Production from Hydrate Bearing Quartz Sediment. Industrial & Engineering Chemistry Research, 52, (2013), 6571-6581.

Hou, J., Xia, Z., Li, S., et al. Operation parameter optimization of a gas hydrate reservoir developed by cyclic hot water stimulation with a separated-zone horizontal well based on particle swarm algorithm. Energy, 96, (2016), 581-591.

Koh, D., Kang, H., Lee, J., et al. Energy-efficient natural gas hydrate production using gas exchange. Applied Energy, 162, (2016), 114-130.

Li, B., Xu, T., Zhang, G., et al. An experimental study on gas production from fracture-filled hydrate by CO2 and CO2/N2 replacement. Energy Conversion and Management, 165, (2018a), 738-747.

Li, G., Moridis, G.J., Zhang, K., et al. Evaluation of gas production potential from marine gas hydrate deposits in Shenhu area of South China Sea. Energy & Fuels, 24, (2010), 6018-6033.

Li, G., Li, X., Zhang, K., et al. Effects of impermeable boundaries on gas production from hydrate accumulations in the Shenhu Area of the South China Sea. Energies, 6, (2013), 4078-4096.

Li, J., Ye, J., Qin, X., et al. The first offshore natural gas hydrate production test in South China Sea. China Geology, 1, (2018b), 5-16.

Li, X., Xu, C., Zhang, Y., et al. Investigation into gas production from natural gas hydrate: A review. Applied Energy, 172, (2016), 286-322.

Liu, Y., Hou, J., Zhao, H., et al. A method to recover natural gas hydrates with geothermal energy conveyed by CO2. Energy, 144, (2018), 265-278.

Lu, N., Hou, J., Liu, Y., et al. Revised inflow performance relationship for productivity prediction and energy evaluation based on stage characteristics of Class III methane hydrate deposits. Energy, 189, (2019), 116211.

Moridis, G., Kowalsky, M., Pruess, K. HydrateResSim Users Manual: A Numerical Simulator for Modeling the Behavior of Hydrates in Geologic Media. Earth Sciences Division, Lawrence Berkeley National Laboratory, Berkeley, CA, 94720, (2005).

Moridis, G., Silpngarmlert, S., Reagan, M., et al. Gas production from a cold, stratigraphically-bounded gas hydrate deposit at the Mount Elbert Gas Hydrate Stratigraphic Test Well, Alaska North Slope: Implications of uncertainties. Marine and Petroleum Geology, 28, (2011), 517-534.

Moridis, G.J. Numerical studies of gas production from methane hydrates. SPE Gas Technology Symposium: Society of Petroleum Engineers; 2002.

Moridis, G.J., Sloan, E.D. Gas production potential of disperse low-saturation hydrate accumulations in oceanic sediments. Energy Conversion and Management, 48, (2007), 1834-1849.

Reagan, M.T., Moridis, G.J., Johnson, J.N., et al. Field-scale simulation of production from oceanic gas hydrate deposits. Transport in Porous Media, 108, (2015), 151-169.

Sloan, E.D. Fundamental principles and applications of natural gas hydrates. Nature, 426, (2003), 353-359.

Sun, J., Ning, F., Li, S., et al. Numerical simulation of gas production from hydrate-bearing sediments in the Shenhu area by depressurising: the effect of burden permeability. Journal of Unconventional Oil and Gas Resources, 12, (2015), 23-33.

Sun, X., Luo, T., Wang, L., et al. Numerical simulation of gas recovery from a low-permeability hydrate reservoir by depressurization. Applied Energy, 250, (2019), 7-18.

Terzariol, M., Goldsztein, G., Santamarina, J. Maximum recoverable gas from hydrate bearing sediments by depressurization. Energy, 141, (2017), 1622-1628.

Xu, C., Li, X. Research progress on methane production from natural gas hydrates. RSC Advances, 5, (2015), 54672-54699.

Yang, M., Fu, Z., Zhao, Y., et al. Effect of depressurization pressure on methane recovery from hydrate–gas–water bearing sediments. Fuel, 166, (2016), 419-426.

Yang, S., Lang, X., Wang, Y., et al. Numerical simulation of Class 3 hydrate reservoirs exploiting using horizontal well by depressurization and thermal co-stimulation. Energy Conversion and Management, 77, (2014), 298-305.

Ye, J.l., Qin, X.w., Xie, W., et al. Main progress of the second gas hydrate trial production in the South China Sea. Geology in China, 47, (2020), 557-568.

Yin, Z., Moridis, G., Tan, H.K., et al. Numerical analysis of experimental studies of methane hydrate formation in a sandy porous medium. Applied Energy, 220, (2018a), 681-704.

Yin, Z., Moridis, G., Chong, Z.R., et al. Numerical analysis of experimental studies of methane hydrate dissociation induced by depressurization in a sandy porous medium. Applied Energy, 230, (2018b), 444-459.

Zheng, Ruyi, Li, et al. Sensitivity analysis of hydrate dissociation front conditioned to depressurization and wellbore heating. Marine & Petroleum Geology, (2018).